

Electrodeposition of CuNiW alloys: thin films, nanostructured multilayers and nanowires

M. Gupta · E. J. Podlaha

Received: 2 July 2009 / Accepted: 27 March 2010 / Published online: 11 April 2010
© Springer Science+Business Media B.V. 2010

Abstract Electrodeposition operating conditions were determined for the deposition of copper–nickel–tungsten alloys and compositionally, multilayered deposits. Multilayered alloys with one layer rich in Cu and the other layer rich in NiW were fabricated as both thin films and nanowires. The electrolyte contained 0.6 M $\text{Na}_3\text{C}_6\text{H}_5\text{O}_7$, 0.2 M Na_2WO_4 , 0.3 M NiSO_4 and variable CuSO_4 concentration at a pH of 8 adjusted with ammonium hydroxide at $70 \pm 2^\circ\text{C}$. The deposit composition and current efficiency were characterized using rotating cylinder electrodes with and without a Hull configuration. Addition of Cu(II) to the electrolyte lowered the tungsten partial current density and hence the W wt% in the deposit. Thin film multilayered alloys, with a modulation in composition, were fabricated with pulse current deposition and conditions to selectively etch one layer was determined with a view towards fabricating nanotemplates. Nanowires with modulated composition were also demonstrated, electrodeposited into alumina nanoporous templates. However, the nanowire deposition was confounded by the formation of oxide during the modulation, and results herein recommend that the potential of the more noble step be more negative than -0.9 V versus SCE to avoid this situation, despite metallic alloy formation in un recessed electrodes.

Keywords CuNiW alloy electrodeposition · Compositionally modulated multilayers · Nanowires

M. Gupta
Cain Department of Chemical Engineering, Louisiana State University, Baton Rouge, LA 70803, USA

E. J. Podlaha (✉)
Department of Chemical Engineering, Northeastern University, Boston, MA 02132, USA
e-mail: e.podlaha-murphy@neu.edu

1 Introduction

Electrodeposition of tungsten alloys are of interest because of their superior properties such as hardness, wear resistance, thermal resistance and corrosion resistance [1–4]. In addition, their electrodeposition behavior is unique since tungsten cannot be deposited from an aqueous electrolyte, nonetheless it can readily be deposited in the presence of iron group metal ions such as cobalt, nickel, and iron [5, 6]. This type of electrodeposition is known as ‘induced co-deposition’ a term coined by Brenner [5]. The present work utilizes tungsten codeposition with both nickel and copper to form a ternary alloy for the fabrication of multilayers.

Multilayered alloys are materials in which the composite of alternative layers is modulated. Since copper is more noble than nickel or tungsten it can be preferentially deposited as one layer. Nickel and tungsten are chosen as the other components of the bilayer in a multilayer stack due to the superior properties of its alloy [3–5, 7–9], and they are typically deposited from ammonia containing electrolytes. Due the presence of ammonia in the baths, the reversible potential of copper is moved to a more negative potential range [10], hindering the ability to form multilayers. Without ammonia, there is a larger separation of the reversible potential of copper and nickel–tungsten, that facilitates multilayer fabrication, however a lower ammonia concentration or no ammonia, lowers the current efficiency appreciably for nickel–tungsten codeposition [11].

Electrodeposition of multilayers is a cost effective and versatile method for developing a wide variety of micro-devices [12–14]. Electrodeposited multilayers have already been applied to many sectors such as electronics, aerospace, automotive, etc. due to low cost and straightforward implementation. There have been many studies on multilayer deposition due to a significant improvement in

electrical properties [15–18], magnetic properties [15, 19–24] and mechanical properties such as hardness [22, 25–28] and tensile strength [19, 22, 27, 29–31].

Electrodeposition of multilayers followed by preferential etching of sacrificial layers can potentially be used as an inexpensive alternative stamp for nanoimprint lithography (NIL) [32–37] applications. NIL has already been shown to find potential applications in bio-chemical analysis systems [34, 37], electronic storage media [34] and optical elements [37, 38] and CD/DVD optical pick up units [39]. It can also be used for fabricating in-fiber gratings in optical fibers [38]. Other applications of electrodeposited multilayers followed by selective etching of one layer are in fabricating micro-electro-mechanical devices such as microgears [14] and liquid-core waveguides [40]. For example, electrodeposited multilayers have recently been demonstrated to fabricate nanostamps using Cu/Ni, Cu/NiFe and CoFeNiCu/Cu systems [41, 42]. The present work includes tungsten in one bilayer to create a more robust nanostamp.

A non-destructive method of visualizing multilayers is to electrodeposit multilayered nanowires and examine them using TEM. Electrodeposition of nanowires has become an attractive field since the inception of GMR (giant magnetoresistance) [20, 23, 43]. The properties of nanowires depend on electrolyte composition, temperature, pH, and applied potential/current. When single layer thickness in nanowires is only a few nanometers, the nanowires exhibit a great decrease in electrical resistance when an external magnetic field is applied. For GMR purposes they consist of alternative layers of ferromagnetic metals such as Ni, Co, Fe or their alloys and paramagnetic metals such as Cu. There are several techniques to fabricate magnetic multilayers such as molecular beam epitaxy (MBE), thermal evaporation and ion beam sputtering [21]. Nonetheless, electrodeposition is a cost effective alternative with other advantages such as simplicity of method and high throughput. To the best of our knowledge, this is the first time CuNiW multilayered nanowires have been fabricated, complimenting the different types of nanowires reported in the literature (e.g., [44–47]).

2 Experimental

2.1 Electrodeposition characterization

2.1.1 Electrolytes

Electrolytes used in all the experiments contained 0.6 M $\text{Na}_3\text{C}_6\text{H}_5\text{O}_7$, 0.2 M Na_2WO_4 , 0.3 M NiSO_4 and varying amount of CuSO_4 . All the chemicals were certified A.C.S. The electrolyte solutions were prepared using deionized

water. The electrolyte temperature was maintained at $70 \pm 2^\circ\text{C}$. NH_4OH was added to the electrolytes, 2.0, 1.5, 1.4% (v/v), containing 0.03, 0.01 and 0.003 M CuSO_4 , respectively to establish the initial pH of 8.0 ± 0.2 , and the pH was maintained by periodically adding NH_4OH between experiments. Experiments were performed using a rotating cylinder electrode (RCE) with a uniform current distribution, a rotating cylinder hull cell (RCHC) with a non-uniform current distribution (Fig. 1) and a rotating disk electrode (RDE) to obtain flat alloy deposits.

2.1.2 Rotating cylinder electrode (RCE) and rotating cylinder hull cell (RCHC)

The RCE and RCHC were used as cathodes with a controlled rotation rate to facilitate a constant hydrodynamic environment near the electrode surface. The electrode materials were a 410 stainless steel (area = 15 cm^2) cylinder surrounded by a platinized, titanium counter electrode. The RCE, with a uniform current distribution along its length, was used to obtain current–potential relationships (polarization curves) at a constant rotation rate. The RCHC, with an induced current distribution, shown in Fig. 1, was used to assess the effect of the applied current density on the deposit composition, thickness and partial current densities. The difference between RCE and RCHC set-up is that the former does not have a plastic shield around the cylindrical cathode. The absence of the shield promotes a uniform current distribution.

The Hull cell configuration, with the shield, is designed in such a way that current varies along the length of the cylinder when the total current rises rapidly with potential. Under these conditions, the current distribution is greatest due to the geometry and the ohmic limitations of the electrolyte, referred to as primary current distribution. The lower end of the cylinder has the highest current density and it decreases along the electrode length. Figure 2

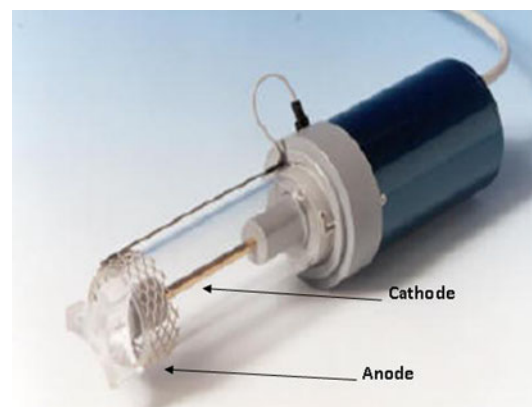


Fig. 1 Rotating cylinder hull cell (RCHC), <http://yanco.com.tr/products/Eco%20Chemie/rotahull.pdf>

presents the current density, i , variation, normalized to the average applied current density, i_{avg} , along the cylindrical cathode length, x , in a RCHC [48], shown as a normalized parameter with the total electrode length, L . The anode is closest to the cathode at $x L^{-1} = 0$, where the current density is at a maximum. The calculated points in Fig. 2 represent a primary current distribution. If the reactions are sluggish then the distribution will be smaller.

After obtaining electrodeposition conditions for different alloys, these were used to estimate conditions to deposit multilayered alloys onto a rotating disc electrode (RDE) and into nanoporous membranes.

2.1.3 Rotating disc electrode (RDE)

Alloys were deposited using a rotating disc electrode (RDE) with a high precision rotator supplied by Pine Instrument Company, Grove City, USA, and electrodeposited under pulsed current conditions. A single compartment cell was used with 410 stainless steel working electrodes (area = 0.28 cm^2), a Pt counter electrode and a saturated calomel reference. Experiments were performed using an IM-6e potentiostat/galvanostat/impedance spectrometer supplied by BAS Zahner.

The cell was kept inside a water bath to maintain the required temperature. Before experiments the cylindrical pellet was cleaned by soap and rinsed with deionized water. The working electrode was a cylindrical pellet having an area of 0.283 cm^2 . The pellet was polished using a 4000 sand paper followed by $3 \mu\text{m}$ diamond spray (Struers).

Linear sweep voltammetry was done to obtain polarization curves for different electrolytes using an IM-6e Potentiostat/Function generator/FRA. A slow scan rate of 2 mV s^{-1} was applied to all scans in order to ensure steady state conditions. Impedance spectroscopy was done to find

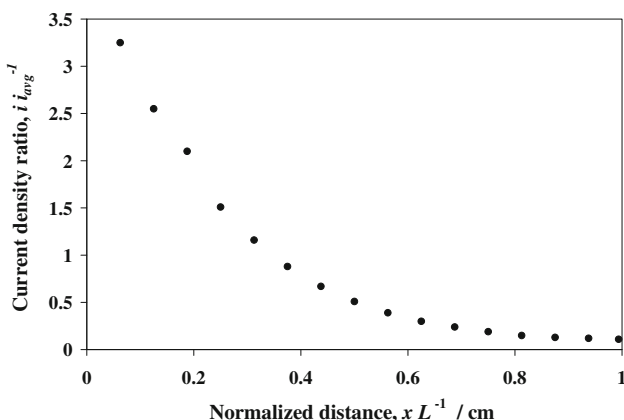


Fig. 2 Normalized current distribution along the cylindrical electrode in a RCHC [48]

solution resistance (ohmic drop) by varying the frequency of 1 kHz to 1 MHz. The ohmic drop was then applied to all polarization curves.

Alloy deposits were obtained at several current densities to obtain varying amount of Cu, Ni, and W suitable for multilayer deposition under normal and pulse plating conditions. The deposits were sufficiently thick (more than $0.5 \mu\text{m}$) to carry out composition analysis.

2.2 Multilayer electrodeposition and etching

All multilayers were electrodeposited using a rotating disc electrode under pulsed current conditions. Table 1 shows the copper, nickel, tungsten and sodium citrate compositions of electrolytes used and the current densities used for alloy and multilayer deposition. The etching solution to preferentially etch one layer of the CuNi/CuNiW multilayers was $0.034 \text{ M K}_2\text{Cr}_2\text{O}_7$, $0.36 \text{ M H}_2\text{SO}_4$, 0.012 M HCl [44].

2.3 Nanowire electrodeposition

Figure 3 shows a schematic of nanowire fabrication using a membrane. The nanowires were electrodeposited into alumina membranes (Whatman Anodisc[®]) having a pore length and diameter of $60 \mu\text{m}$ and 200 nm , respectively. The membranes were gold sputtered on one side for electrical contact. The gold sputtered membrane and a platinum mesh served as cathode and anode, respectively. The electrolyte contained $0.6 \text{ M Na}_3\text{Cit}$, $0.2 \text{ M Na}_2\text{WO}_4$, 0.3 M NiSO_4 and 0.03 M CuSO_4 (solution A). Temperature and pH were $70 \pm 2^\circ\text{C}$ and 8.0 ± 0.2 , respectively. Other experimental variables are given in Table 2. The potentials shown in the following table are chosen corresponding to the current densities values for multilayer deposition.

2.4 Characterization

The compositional analyses of the films deposited on the cylinder electrodes were measured by energy dispersive X-Ray Fluorescence (XRF), model Omicron by Kevex.

Table 1 Electrolytes and corresponding current densities used for multilayer deposition

Electrolyte	CuSO ₄	Ni-rich (mA cm^{-2})	Cu-rich (mA cm^{-2})
A	0.03 M	-35.38	-7.08
B	0.01 M	-35.38	-1.76
C	0.003 M	-35.38	-0.71

A: $0.6 \text{ M Na}_3\text{C}_3\text{H}_5\text{O}(\text{CO}_2)_3$, $0.2 \text{ M Na}_2\text{WO}_4$, 0.3 M NiSO_4 and 0.03 M CuSO_4 ; B: $0.6 \text{ M Na}_3\text{C}_3\text{H}_5\text{O}(\text{CO}_2)_3$, $0.2 \text{ M Na}_2\text{WO}_4$, 0.3 M NiSO_4 and 0.01 M CuSO_4 ; C: $0.6 \text{ M Na}_3\text{C}_3\text{H}_5\text{O}(\text{CO}_2)_3$, $0.2 \text{ M Na}_2\text{WO}_4$, 0.3 M NiSO_4 and 0.003 M CuSO_4

The XRF analyses were performed at an X-ray energy of 50 kV, current of 1.7 mA and acquisition time of 100 s. Multilayer characterization (a few microns to submicron size), was carried out by a scanning electron microscope (model JSM-840A) and a transmission electron microscope (model JEOL 100CX), manufactured by JEOL.

3 Results and discussion

3.1 Electrodeposition characterization

3.1.1 Rotating cylinder electrode (RCE)

Figure 4 shows the polarization curves of the electrolytes containing different amounts of copper obtained using the RCE at a rotation rate of 400 rpm. The plateau region of the curves (-0.6 to -0.8 V vs. SCE) that increase with copper in the electrolyte indicate the region where the Cu limiting current density occurs. At potentials more noble to this region, the deposits are copper while at less noble potentials deposits are an alloy containing nickel, copper and tungsten. The composition, thickness and resulting partial current densities were determined by using the RCHC.

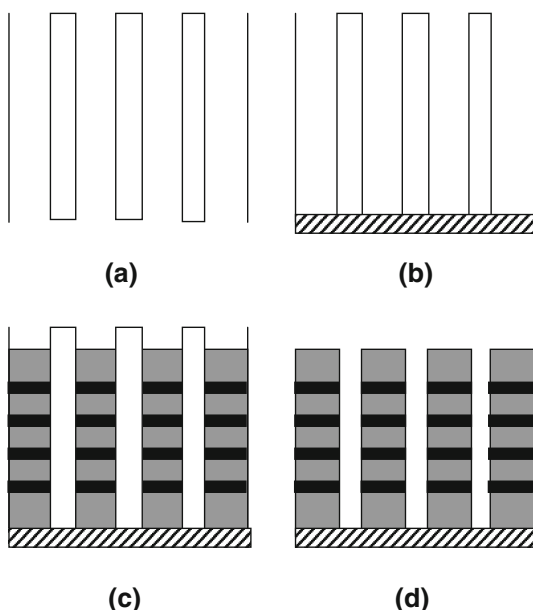


Fig. 3 Schematic for nanowires fabrication **a** cross-sectional view of cylindrical pores in an alumina membrane, **b** sputtered gold on membrane bottom surface, **c** filled pores with electrodeposited multilayered structure, and **d** multilayered nanowires protruding from gold layer after dissolution of membrane in 1 M KOH

Table 2 Electrolytes and corresponding applied potential for nanowires electrodeposition

Electrolyte	CuSO ₄	NiW-rich (−V vs. SCE)	Cu-rich (−V vs. SCE)
A	0.03 M	1.4–1.8	0.6–0.9
C	0.003 M	1.4–1.8	0.6–0.9

3.1.2 Rotating cylinder hull cell (RCHC)

Guided by the polarization curves in Fig. 4, the applied average current density to the RCHC was $-13.33 \text{ mA cm}^{-2}$ and resulted in a deposit that varied in composition along the electrode length. Figure 5a shows the variation of copper along the length of the cylinder, expressed in terms of the estimated applied current density. The copper content in the alloy increases with copper in the solution and decreases with the applied current density consistent with a mass transport control. When copper is decreased from 0.03 to 0.01 M the copper content in the alloy decreases by 40 wt%, and it is reduced by 62 wt% when the copper concentration is further decreased to 0.003 M at lower current density. The nickel content in the alloy is always higher than tungsten for all the electrolytes (Fig. 5b, c). The amount of tungsten increases slightly with an increase in current density and the amount of nickel stays about the same. Figure 5b and c also shows that the nickel and tungsten content in the alloy decreases with more copper in the system as expected. At lower current densities, the difference in the nickel content from the different solutions is more than at the higher current densities. The amount of tungsten in the alloy is high at higher current densities consistent with other literature studies [5]. The highest amount of tungsten achieved was 31 wt% from electrolyte containing 0.003 M Cu(II).

In an attempt to better understand the system and the interaction among all species, the partial current densities

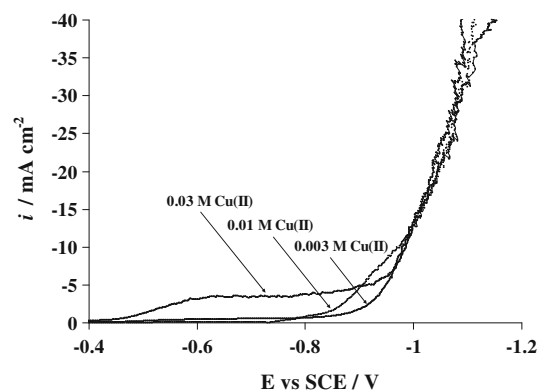


Fig. 4 Ohmic drop corrected polarization curves with rotating cylinder electrodes (rpm = 400) from electrolytes having different Cu ion concentrations

were determined and expressed as a function of potential. The partial current density i_k (mA cm^{-2}) of k th species in the electrolyte is calculated as

$$i_k = \frac{(1000)(X_k)(n_k)(m)(F)}{(AW_k)(t)} \quad (1)$$

where k represents copper, nickel and tungsten, X_k is the weight fraction, n_k (eq mol^{-1}) is the number of electrons involved in balanced equation for reduction, m (g cm^{-2}) is

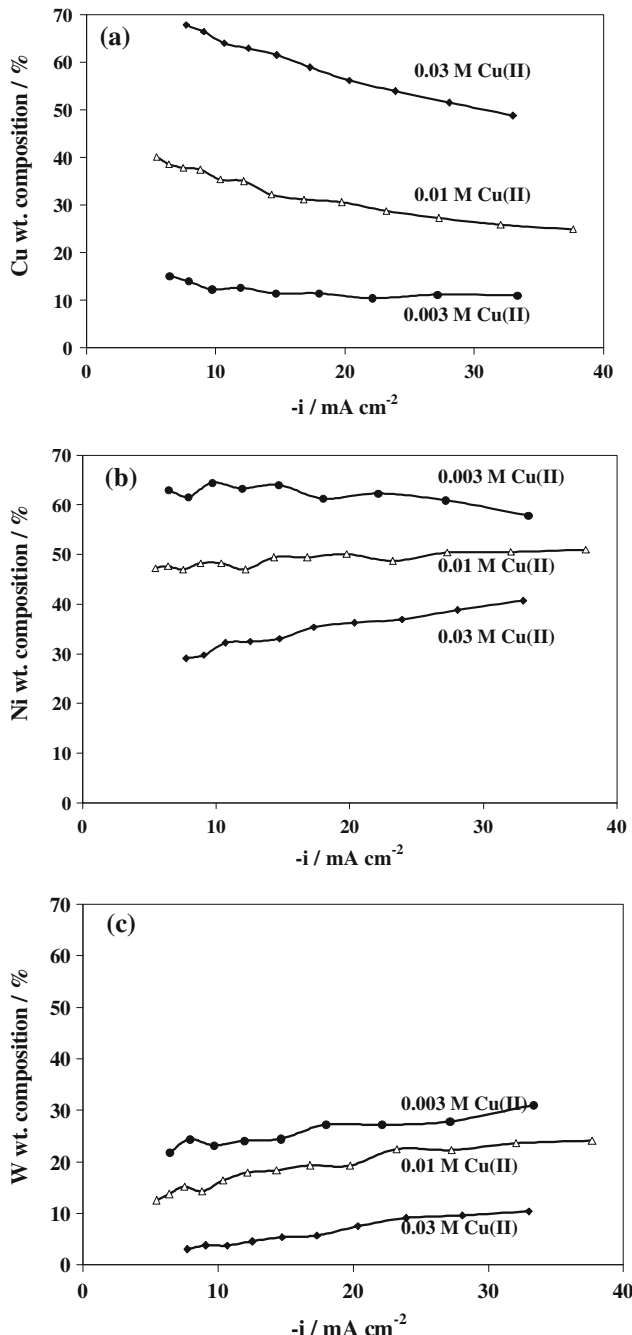


Fig. 5 Deposit composition **a** Cu, **b** Ni, and **c** W in the CuNiW alloy deposited from electrolytes having different Cu ion concentrations

the total mass deposited per unit area, F (96485 C eq^{-1}) is the Faraday's constant, AW_k (g mol^{-1}) is the atomic weight and t (s) is the total electrodeposition time. The mass per unit area, m is determined from the thickness measurement.

$$m = \frac{\theta}{(X_{\text{Cu}}/\rho_{\text{Cu}}) + (X_{\text{Ni}}/\rho_{\text{Ni}}) + (X_{\text{W}}/\rho_{\text{W}})} \quad (2)$$

where θ (cm) is the thickness of the deposit and ρ_{Cu} , ρ_{Ni} , and ρ_{W} are the densities of copper, nickel and tungsten, respectively.

The side reaction is defined as

$$i_s = i_{\text{Total}} - (i_{\text{Cu}} + i_{\text{Ni}} + i_{\text{W}}) \quad (3)$$

where i_{Total} is the total current applied and i_{Cu} , i_{Ni} and i_{W} are partial current densities of copper, nickel and tungsten, respectively. Current efficiency is determined from the ratio of the metal partial current densities to the total current density applied.

Figure 6a–c represents the calculated partial current densities determined from measured composition and thickness data plotted against an interpolated potential from the polarization curves (Fig. 4). In Fig. 6a the partial current density of copper is highest for the electrolyte containing 0.03 M Cu(II) and lowest for the electrolyte with 0.003 M Cu(II), as expected for a mass transport control. Although, at the highest amount of Cu(II), 0.03 M, there is evidence of a mixed kinetic control since the partial current increases with potential. The negligible change of the partial current density with potential of copper from the dilute electrolytes clearly indicates a mass transport control. The partial current density of nickel (Fig. 6b) for all the electrolytes, increases when potential becomes more negative, indicating kinetic control. The nickel partial current densities are almost the same up to -1 V . For the potentials more negative than -1 V , it increases as the copper content in the electrolyte increases, this trend is consistent with past study of Cu–Ni codeposition in citrate electrolyte [45]. Figure 6c depicts the tungsten partial current density, which is lowest for the electrolyte containing the highest amount of copper. The addition of copper in the electrolyte thus affects the tungsten partial current density.

The side reaction is primarily H_2 evolution which becomes more favorable at higher negative potentials as shown in Fig. 7a. The side reaction was significantly reduced in the whole range of potential with the addition of copper in the electrolyte. There is no effect on the side reaction when the copper ion concentration is reduced from 0.03 to 0.01 M. However, as the copper electrolyte concentration is reduced to 0.003 M the side reaction increases, accompanied with an increase in tungsten. Another way of representing the same data is in the calculation of the current efficiency, Fig. 7b. The current

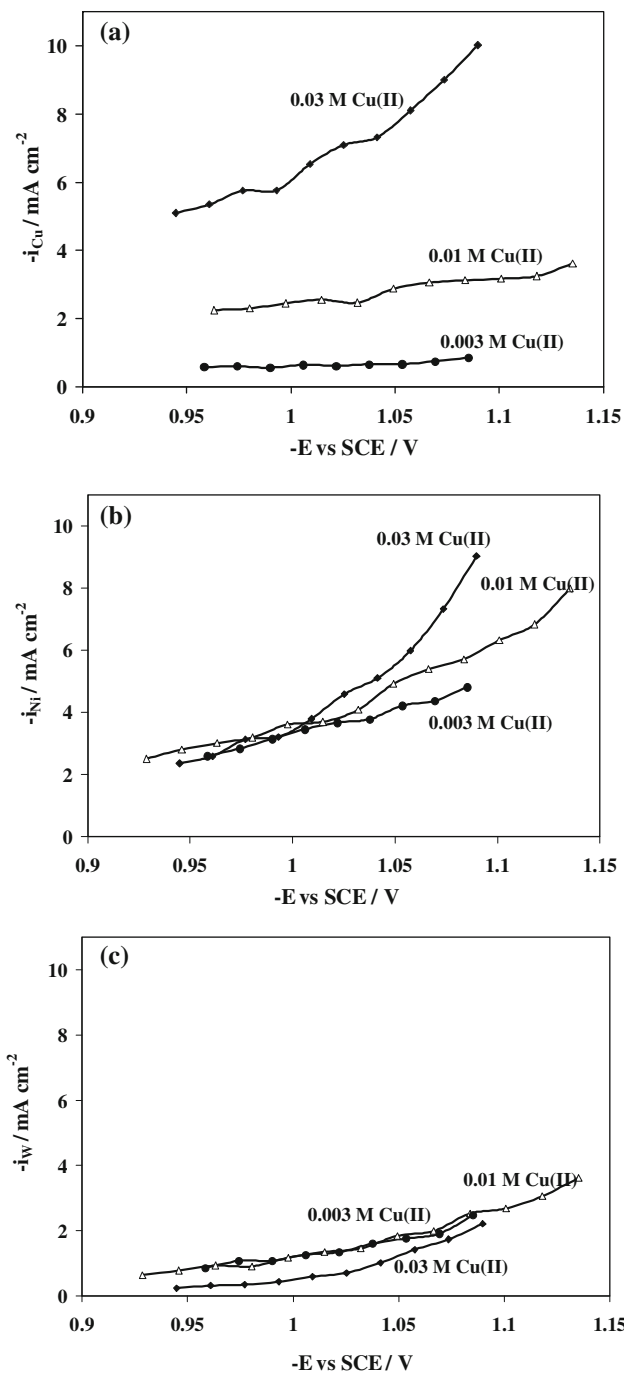


Fig. 6 Partial current densities of **a** Cu, **b** Ni, and **c** W from electrolytes having different Cu ion concentration

efficiency follows the same trend for all the electrolytes, decreasing with the current density. The highest current efficiency occurs with the deposits containing the most amount of copper from 0.03 M Cu(II) and the lowest current efficiency (24%) was recorded from the electrolyte containing the lowest amount of copper (0.003 M Cu(II)).

3.2 Multilayer thin film deposition

3.2.1 Rotating disc electrode (RDE)

The rotating disc electrode was used to create flat deposits using the conditions obtained in the previous section, for multilayer fabrication. Figure 8 shows the ohmic drop (iR) corrected polarization curves for the three electrolytes containing different concentrations of copper at 900 rpm. The curves are qualitatively similar to the polarization curves generated by the RCE (Fig. 4). The compositional analysis of the alloy films from the electrolytes at two applied current densities for multilayer deposition was investigated. The lower current density was chosen to obtain a CuNi alloy in one layer. Since the limiting current density is dependent upon the concentration, the low current density value will vary for the different electrolytes. Approximately the same ratio (0.25) of total current to the limiting current was maintained. At an applied current density of -7.08 , -1.76 and -0.71 mA cm^{-2} , the copper wt% was 95, 97 and 99. At the higher applied current density of $-35.38 \text{ mA cm}^{-2}$ the composition was 59, 26

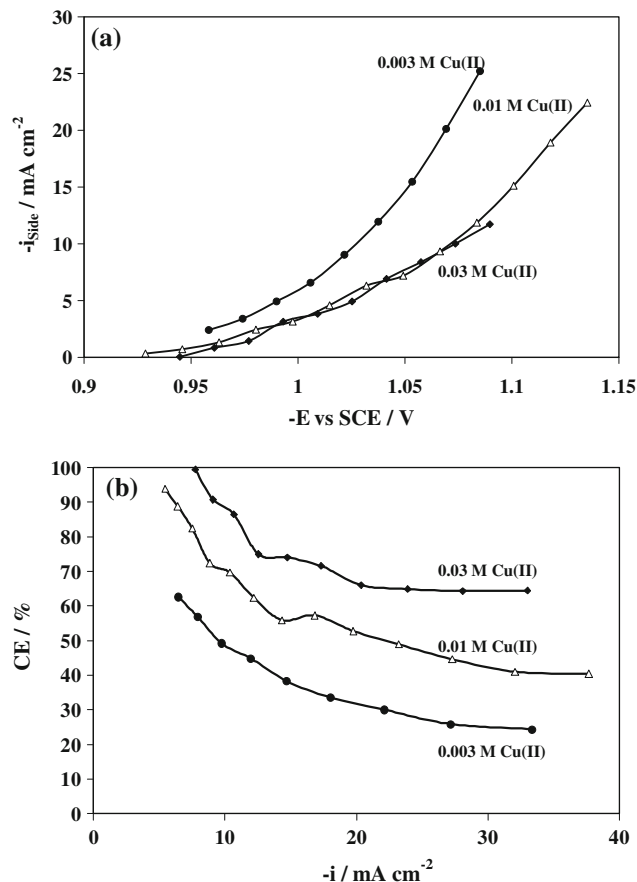


Fig. 7 Side reaction **a** partial current density and resulting **b** current efficiency in electrolytes having different Cu ion concentration

and 11 wt% for copper in the three electrolytes. The nickel and tungsten concentrations were 36, 58, 69 and 5, 16, 19 wt%, respectively.

3.2.2 Etching characteristics

Polarization curves of the Cu-rich and NiW-rich CuNiW alloys were examined to assess the etching characteristics of individual layers during chemical etching in a chromic acid electrolyte. Figure 9a shows the etching of the deposits created from the 0.03 M Cu(II) electrolyte and Fig. 9b from the low 0.003 M Cu(II) electrolyte. The cathodic part of the curves arise from H^+ and O_2 reduction and the anodic part is due to the etching of the deposit. The corrosion current densities and respective corrosion potentials of Cu-rich and NiW-rich deposits are presented in Table 3. Both electrolytes have a higher corrosion current density for Cu-rich deposits indicating that this layer will dissolve at a faster rate than the NiW-rich deposits. The Cu-rich alloy has a less noble corrosion potential than NiW-rich alloys. The larger the difference between the corrosion current densities and potential of the Cu-rich and NiW-rich alloys, the better will be the selectivity of etching. Therefore, the results suggest that multilayers can be preferentially etched, and that the deposit containing the least amount of copper in the NiW-rich alloy side, deposited from the electrolyte containing 0.003 M Cu(II), would be most selectively etched. Differences in the corrosion potential and current density may be attributed to not only the composition changes, but also deposit structure and variability in passivation.

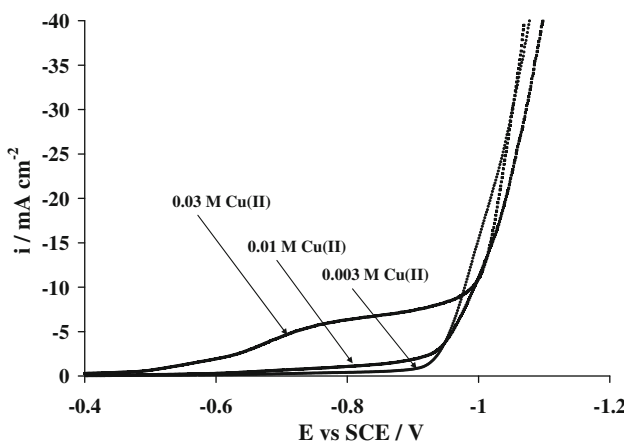


Fig. 8 Ohmic drop corrected polarization curves with a rotating disc electrode (rpm = 900) from electrolytes having different Cu ion concentrations

3.2.3 SEM

Figures 10 and 11 are SEM micrographs of multilayer examples after selective etching of the Cu-rich layer. The Cu-rich layers are darker than the NiW-rich layers. In all the images, layers are deposited from bottom to top. In Fig. 10a Cu-rich (85 ± 32 nm) and NiW-rich (124 ± 25 nm) layers obtained from the electrolyte containing 0.003 M Cu(II) were electrodeposited at -0.71 mA cm^{-2} for 10 min and $-35.38 \text{ mA cm}^{-2}$ for 12 s, respectively. In Fig. 10b the Cu-rich layer (99 ± 18 nm) was deposited at -7.08 mA cm^{-2} for 1 min and NiW-rich (140 ± 16 nm) layer was deposited at $-35.38 \text{ mA cm}^{-2}$ for 15 s from the electrolyte containing 0.03 M Cu(II). A better quality of deposition and etching was observed using the concentrated Cu(II) electrolyte, even though the etching should have been more selective when the layers are electrodeposited from the more dilute Cu(II) solution. Thus, the conditions of electrodeposition are more critical than for etching.

Multilayers in Fig. 11 were deposited at the same current conditions as discussed above but the time of the

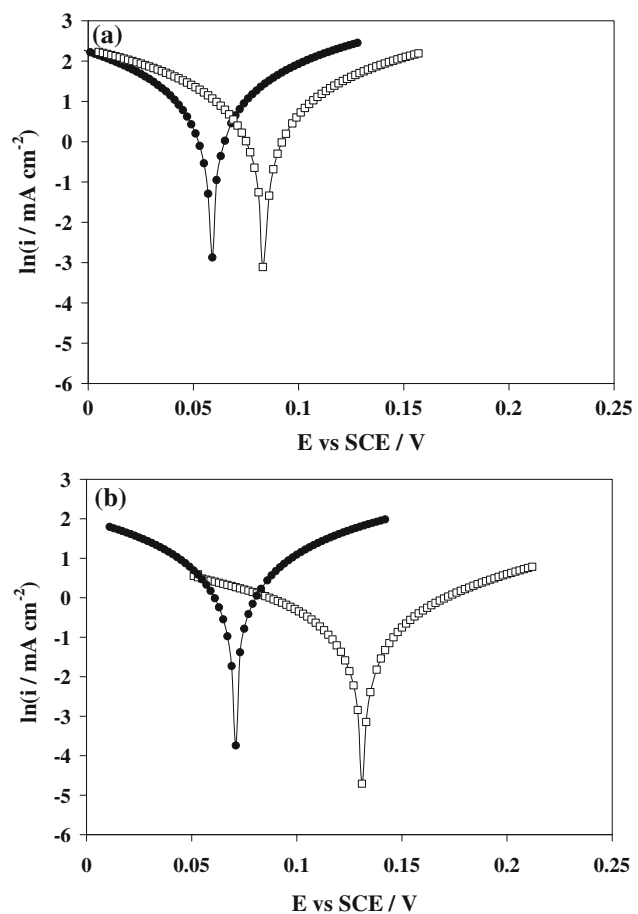
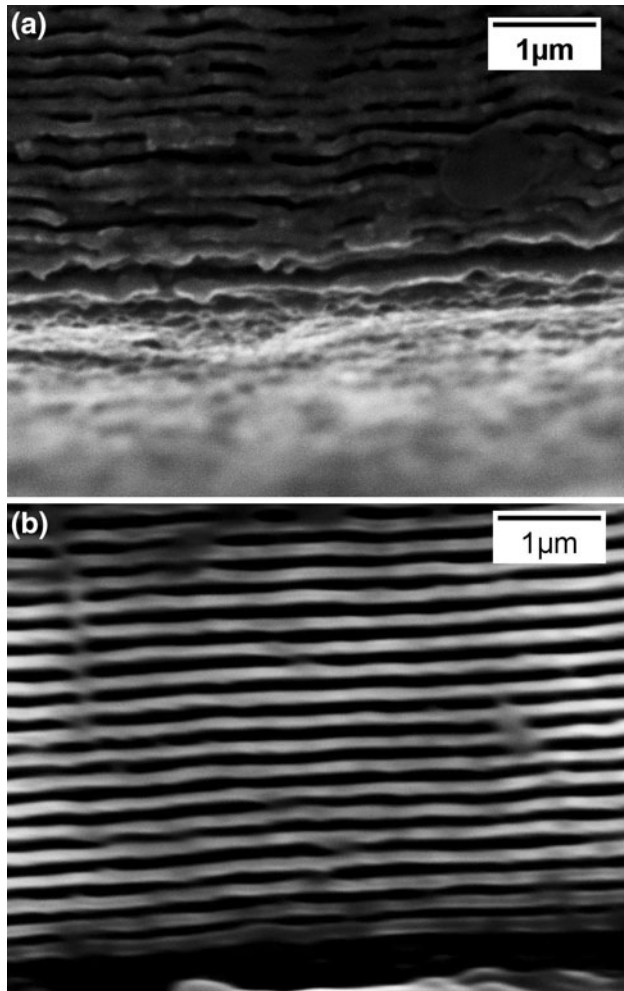
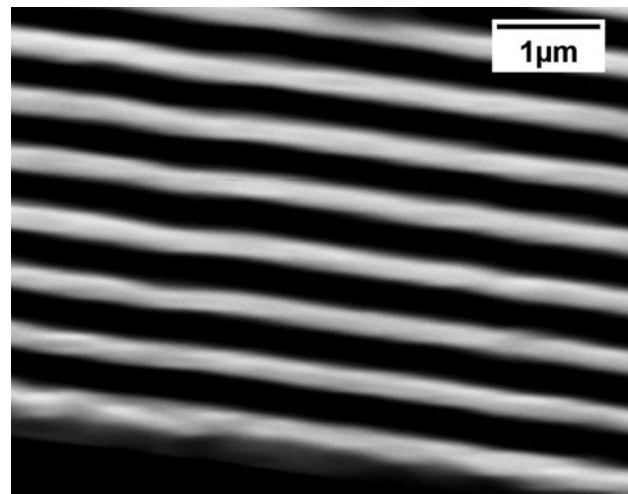


Fig. 9 Polarization curves of Cu-rich deposit (filled circle) and NiW-rich deposit (open square) from **a** electrolyte A (0.03 M Cu(II)) and **b** electrolyte C (0.003 M Cu(II)) during electrochemical etching

Table 3 Corrosion results for various deposits

	Corrosion current density (mA cm^{-2})	Corrosion potential (mV)
Electrolyte A		
CuNi	3.3	59
CuNiW	2.3	83
Electrolyte C		
CuNi	2.7	71
CuNiW	0.5	131

deposition was doubled for both the layers along with the etching time (from 30 s to 1 min). The thicknesses of Cu-rich and NiW-rich layers are 205 ± 13 and 280 ± 19 nm, respectively. The thicknesses of Cu-rich and NiW-rich layers are doubled by doubling the time, consistent with Faraday's law. The multilayered features in all of these images have uniform layers with well defined interfaces. A disadvantage of using the more concentrated electrolyte is that the deposit contains more copper and less tungsten in

**Fig. 10** SEM micrograph of multilayers from **a** electrolyte 0.003 M Cu(II) and **b** electrolyte 0.03 M Cu(II)**Fig. 11** SEM micrograph of multilayers from electrolyte 0.03 M Cu(II)

the NiW-rich layer. However it has been observed that even low amounts of tungsten in a NiW deposit can appreciably increase hardness [47].

3.3 Nanowires

Figure 12 shows the polarization curve for the concentrated Cu(II) electrolyte using the nanoporous template electrode. The plateau reached at potentials more noble than -0.8 V is due to copper's mass transport controlled deposition. Nickel and tungsten deposition start just after -0.8 V and -1.0 V, respectively. Water reduction also occurs after -0.8 V. Therefore, potentials ranging from -0.6 V to -1.0 and -1.0 to -1.8 V were expected to obtain Cu-rich and NiW-rich multilayers, respectively, in a pulsed fashion.

Figure 13a and b presents TEM results of nanowires deposited at -0.7 V for 80 s and -1.3 V for 10 s, where, dark and light layer thicknesses are 77 ± 6 nm and 7 ± 2 nm, respectively (Fig. 13a) and another case when the lower potential is deposited for a longer time, 120 s (Fig. 13b). Figure 14 is another example of nanowires deposited at -0.94 V for 60 s and -1.3 V for 10 s. The

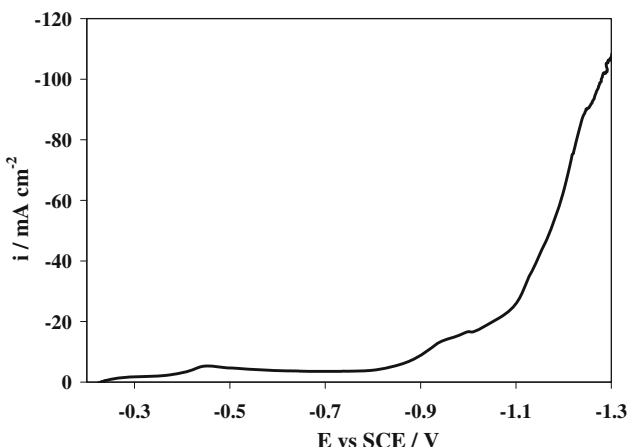


Fig. 12 Ohmic drop corrected polarization curve with an alumina membrane from electrolyte 0.03 M Cu(II)

layer thickness is difficult to measure as the interface is not clear. Inspection of the current transients showed that at potential more positive than -0.93 V the current was positive and hence oxidation took place (Fig. 15), even though at steady state the current was expected to be negative and reductive. Current transients for the pulses between -0.94 V for 60 s and -1.3 V for 10 s, are all negative currents (Fig. 16).

In the region where an oxide can develop, the more positive potential was varied from -0.7 to -0.9 V (maintaining a constant potential and time of -1.3 V , 10 s for the other pulse). Table 4 summarizes the layer thickness results. It was found that the CuNiW alloy (dark) layer thickness increased even at constant higher potential (-1.3 V) and time (10 s), when the lower potential was changed.

It was also observed that an increase in time at the more positive potential did not increase the layer thickness which is consistent with a chemical step controlling the formation of an oxide. Table 5 summarizes these findings. Layer thickness did not increase proportional to time; when time is doubled to 80 s, there was an increase of 17% but when it was further increased to 120 s, no change was observed in thickness. Longer time (120 s) at the lower potential resulted in multilayered features (Fig. 13b). In addition, the pulse nature of the deposit helps to reduce the amount of gas accumulated in the pores. At applied potentials more negative than -1.3 V the pores become blocked by excessive gas evolution.

4 Conclusions

Electrodeposition conditions were evaluated to achieve a disparity in deposit composition and smooth morphology for CuNi and CuNiW deposits. The larger amount of copper ions in the electrolyte lowered the amount of

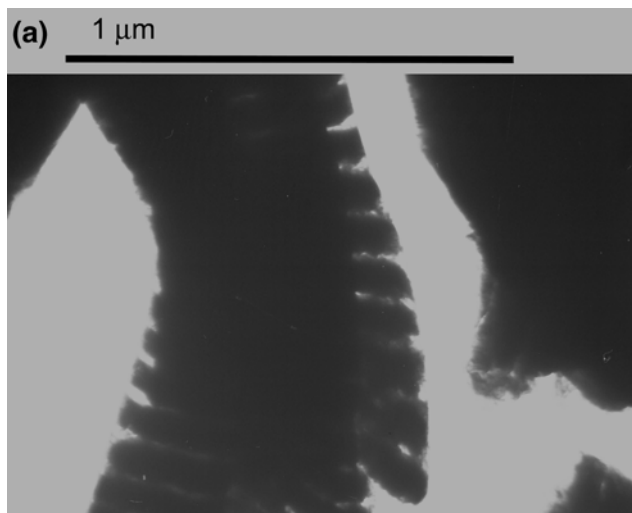


Fig. 13 TEM micrograph of multilayered nanowires: **a** -0.7 V for 80 s and -1.3 V for 10 s, **b** -0.7 V for 120 s and -1.3 V for 10 s

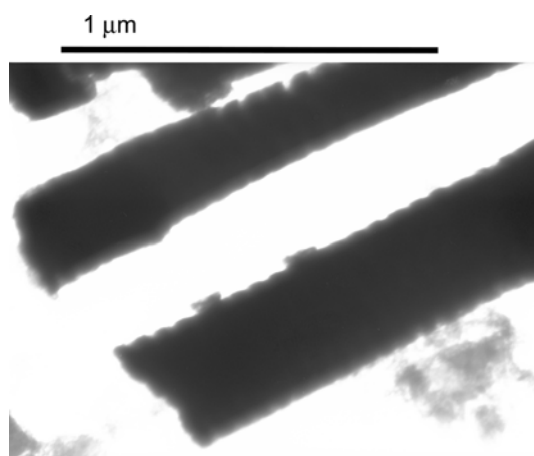


Fig. 14 TEM micrograph of multilayered nanowires, -0.94 V for 60 s and -1.3 V for 10 s

tungsten in the deposit. The current densities of -35.38 and -7.08 mA cm^{-2} were found to be suitable for higher tungsten and copper contents in the alloy, respectively for thin film, multilayer fabrication.

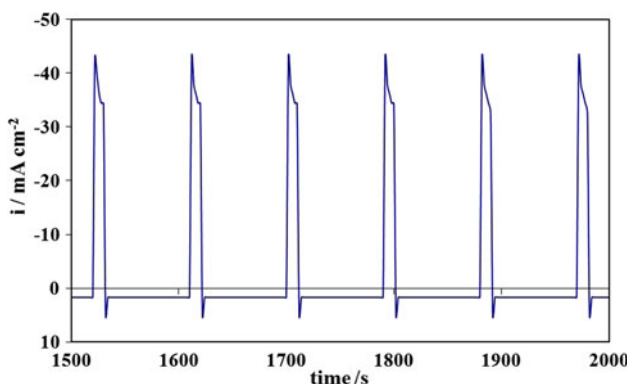


Fig. 15 Current transients during nanowire deposition, -0.7 V for 80 s and -1.3 V for 10 s

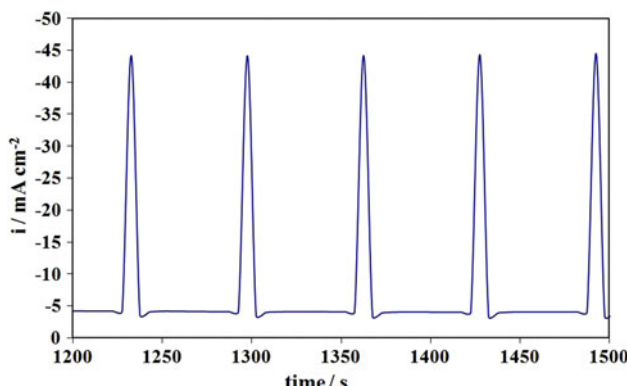


Fig. 16 Current transients during nanowire deposition, -0.94 V for 60 s and -1.3 V for 10 s

Table 4 Effect of lower potential on layer thickness

Sample	Potential (V)	Time (s)	Layer thickness
A	-0.7	40	6 ± 3
	-1.3	10	78 ± 7
B	-0.8	40	5 ± 2
	-1.3	10	91 ± 5
C	-0.9	40	4 ± 1
	-1.3	10	96 ± 9

Table 5 Effect of time on layer thickness

Time (s)	40	80	120
Light layer thickness (nm)	6 ± 2	7 ± 2	7 ± 2
Dark (alloy) layer thickness (nm)	78 ± 7	77 ± 3	60 ± 3

The partial current densities of the metal reaction and side reactions were investigated. The Cu partial current densities increased with more copper in the electrolyte, as expected for a transport control. The Ni partial current densities were under kinetic control and observed to be the same for all three electrolytes up to -1.0 V , and then

decreased as the copper amount in the electrolyte was reduced. The W partial current densities were affected by the addition of copper only when the copper concentration was reduced to 0.01 M from 0.03 M . No effect was observed when the copper concentration was further reduced to 0.003 M . The copper addition in the electrolyte decreased tungsten content in the alloy but improved the current efficiency.

The etching studies of the multilayers showed that the Cu rich-CuNiW deposits etched preferentially compare to the NiW-rich deposits. The etching parameters of bulk Cu-rich and NiW-rich alloys were examined with rotating disk electrodes. The selectivity between the deposits were greater when deposited from electrolytes having less Cu(II) (0.003 M) compared to the electrolytes containing higher Cu(II) concentration (0.03 M), due to a greater disparity in deposit composition. Nevertheless, even a higher selectivity with regard to etching not always resulted in sharp and well defined multilayers. This indicated that the multilayered features were governed by electrodeposition rather than etching.

Multilayered nanowires of CuNiW and its oxide having nanometric scale were deposited for pulse potential conditions: -0.7 V ($x\text{ s}$); -1.3 (10 s) , where the time, x ranged from 40 to 120 s. Increasing this time during the more positive potential, -0.7 V , did not change the layer thickness consistent with a non-metallic deposit, despite having a metallic deposit on rotating electrodes at this potential. Thus, multilayered deposition in this system is confounded by the formation of interfacial oxide at the low potential region and can be avoided by choosing a more negative potential.

Acknowledgements The authors thankfully acknowledge funding from NSF, # 0746567. We would also like to acknowledge Ms. Margaret C. Hank and Dr. X. Xie for their help in TEM and SEM imaging, respectively.

References

- Yao S, Zhao S, Guo H, Kowaka M (1996) Corrosion 52:183
- Singh VB, Singh LC, Tikoo PK (1980) J Electrochim Soc 127:590
- Atanassov N, Gencheva K, Bratoeva M (1997) Plat Surf Finish 84:67
- Obradovic M, Stevanovic J, Despic A, Stevanovic R, Stoch JJ (2001) J Serb Chem Soc 66:899
- Brenner A (1963) Electrodeposition of alloys: principles and practice, vol II: practical and specific information. Academic Press, New York, p 656
- Akiyama T, Fukushima H (1992) ISIJ Int 32:787
- Eliaz N, Sridhar TM, Gileadi E (2005) Electrochim Acta 50:2893
- Yamasaki T (2000) Mater Phys Mech 1:127
- Landa V, Vitek J, Neumann J (1987) Plat Surf Finish 74:128
- Chassaing E, Vu Quang K, Wiart R (1986) J Appl Electrochim 16:591

11. Younes O, Gileadi E (2002) *J Electrochem Soc* 149:C100
12. Arai S, Hasegawa T, Kaneko N (2003) *J Electrochem Soc* 150:C798
13. Arai S, Hasegawa T, Kaneko N (2004) *Electrochim Acta* 49:945
14. Leith SD, Schwartz DT (1999) *J Micromech Microeng* 9:97
15. Myung NV, Nobe K (2000) *Plat Surf Finish* 87:125
16. Krishnan KSR, Srinivasan K, Mohan S (2002) *Trans Inst Met Finish* 80:46
17. Peter L, Kupay Z, Cziraki A, Padar J, Toth J, Bakonyi I (2001) *J Phys Chem B* 105:10867
18. Bakonyi I, Toth-Kadar E, Toth J, Becsei T, Tarnoczi T, Kamasa P (1999) *J Phys Condens Matter* 11:963
19. Ross CA (1994) *Annu Rev Mater Sci* 24:159
20. Osaka T, Asahi T, Kawaji J, Yokoshima T (2005) *Electrochim Acta* 50:4576
21. Alper M (2002) In: Shi D, Aktaç B, Pust L, Mikailov F (eds) *Nanostructured magnetic materials and their applications*, vol 593. Springer, p 111
22. Switzer JA (2001) In: Hodes G (ed) *Electrochemistry of nanomaterials*. Wiley–VCH, p 67
23. Huang Q, Young DP, Chan JY, Jiang J, Podlaha EJ (2002) *J Electrochem Soc* 149:C349
24. Myung NV, Schwartz M, Nobe K (2000) *Proc Electrochem Soc* 99-33:263
25. Blum W (1921) *Trans Am Electrochem Soc* 40:307
26. Donten M, Stojek Z (1996) *J Appl Electrochem* 26:665
27. Foecke T, Lashmore DS (1992) *Scr Metall Mater* 27:651
28. Barnett SA, Shinn M (1994) *Annu Rev Mater Sci* 24:481
29. Gabe DR, Wilcox GD (2002) *Met Finish* 100:18
30. Tench DM, White JT (1984) *Metall Trans A* 15A:2039
31. Tench DM, White JT (1991) *J Electrochem Soc* 138:3757
32. Maximov I, Sarwe EL, Beck M, Deppert K, Graczyk M, Magnusson MH, Montelius L (2002) *Microelectron Eng* 61–62:449
33. Cao H, Yu Z, Wang J, Tegenfeldt JO, Austin RH, Chen E, Wu W, Chou SY (2002) *Appl Phys Lett* 81:174
34. Miyauchi A (2005) *J Photopolym Sci Technol* 18:523
35. Luesebrik H, Glinsner T, Jakeway SC, Crabtree HJ, Cameron NS, Roberge H, Veres T (2005) *J Nanosci Nanotechnol* 5:864
36. Chou SY, Krauss PR, Zhang W, Guo L, Zhuang L (1997) *J Vac Sci Technol B* 15:2897
37. Hirai Y, Tanaka Y (2002) *J Photopolym Sci Technol* 15:475
38. Jackman RJ, Whitesides GM (1999) *Chemtech* 5:18
39. Wang JJ, Chen L, Tai S-W, Deng X, Sciotino PF, Liu F, Deng J, Liu X, Nikolov A, Sinatore D (2005) *Proc SPIE* 5592:51
40. Schueler OJA, Zhao X-M, Whitesides GM, Smith SP, Prentiss M (1999) *Adv Mater* 11:37
41. Lim C-Y, Huang Q, Xie X, Safir A, Harfenist SA, Cohn R, Podlaha EJ (2004) *J Appl Electrochem* 34:857
42. Huang Q, Podlaha EJ (2005) *J Appl Electrochem* 35:1127
43. Bozzini B, Giovannelli G, Lecis N, Lenardi C, Magagnin L, Manara D, Negri E, Vallauri R, Zangari G (1999) *AIFM Galvanotecnica e Nuove Finiture* 9:256
44. Bradley PE, Landolt D (1999) *Electrochim Acta* 45:1077
45. Heydon GP, Hoon RS, Farley AN, Tomlinson SL, Valera MS, Attenborough K, Schwarzacher W (1997) *J Phys D Appl Phys* 30:1084
46. Evans PR, Yi G, Schwarzacher W (2000) *Appl Phys Lett* 76:481
47. Piraux L, Dubois S, Duvail JL, Ounadjela K, Fert A (1997) *J Magn Magn Mater* 175:127
48. Eco Chemie, Inc. The Netherlands. <http://www.autolab-instruments.com>